Molecular Vision 2011; 17:1222-1230 <http://www.molvis.org/molvis/v17/a137>
Received 26 September 2010 | Accepted 1 May 2011 | Published 6 May 2011

Transcriptional factors associated with epithelial-mesenchymal transition in choroidal neovascularization

Manabu Hirasawa,[1,2] Kousuke Noda,[1,3] Setsuko Noda,[4] Misa Suzuki,[1,5] Yoko Ozawa,[1,2] Kei Shinoda,[6] Makoto Inoue,[7] Yoko Ogawa,[2] Kazuo Tsubota,[2] Susumu Ishida[1,2,3]

[1]Laboratory of Retinal Cell Biology, Keio University School of Medicine, Tokyo, Japan; [2]Department of Ophthalmology, Keio University School of Medicine, Keio University School of Medicine, Tokyo, Japan; [3]Department of Ophthalmology, Hokkaido University Graduate School of Medicine, Sapporo, Japan; [4]Department of Nursing, Tokai University School of Health Sciences, Isehara, Japan; [5]Department of Ophthalmology and Visual Science, Yokohama City University Graduate School of Medicine, Yokohama, Japan; [6]Department of Ophthalmology, Teikyo University School of Medicine, Tokyo, Japan; [7]Kyorin Eye Center, Kyorin University School of Medicine, Tokyo, Japan

Purpose: To investigate the transcriptional factors associated with epithelial-mesenchymal transition (EMT) in choroidal neovascularization (CNV) secondary to age-related macular degeneration (AMD).

Methods: Paraffin sections of CNV obtained from patients with AMD (n=12) were stained for transcriptional factors related to EMT, *i.e.*, Snail, Slug, SIP1, and Twist. As a control, postmortem sections of ocular normal tissue were used. Furthermore, using a human retinal pigment epithelial (RPE) cell line (ARPE-19), reverse transcription–polymerase chain reaction (RT–PCR) and immunofluorescence microscopy were performed to explore the cellular localization and expression levels of EMT-associated transcriptional factors upon cytokine stimulation.

Results: Of 12 specimens, 11 CNV tissues (91.6%) showed staining for Snail localized in cellular nuclei, particularly in those of RPE cells. Snail was strongly co-localized with α-smooth muscle antigen (SMA) in RPE cells. In contrast, postmortem human retina showed no Snail staining in RPE cells. Other transcriptional factors, Slug, Twist and SIP1 were not detected in CNV or normal human retina. In ARPE-19 cells, RT–PCR and immunofluorescence microscopy showed that Snail mRNA was upregulated by transforming growth factor (TGF)-β and VEGF stimulation. Furthermore, TGF-β induced relocalization of Snail to the nucleus in RPE cells.

Conclusions: The current data indicate that Snail is a major transcriptional factor for EMT changes of RPE cells in human CNV.

Wet age-related macular degeneration (AMD), characterized by the formation of choroidal neovascularization (CNV), is a leading cause of irreversible blindness among people over age 50 in the western world [1]. So far, the mechanisms of CNV formation have been well analyzed, and lines of evidence have revealed that angiogenesis, inflammation, and oxidative stress are the underlying causes [1-7]. The accumulated data have led to the development of several therapeutic strategies for AMD, such as verteporfin photodynamic therapy (PDT) [8], anti-vascular endothelial growth factor (VEGF) therapy [9], and combined therapy [10,11]. By contrast, little is known regarding the molecular mechanism(s) of tissue scar formation in CNV. Since fibrotic changes in the foveal CNV lesion result in permanent visual impairment in patients with wet AMD [12], the mechanisms of tissue fibrosis in the late stage of AMD are of great interest.

Correspondence to: Kousuke Noda, M.D., Ph.D., Department of Ophthalmology, Hokkaido University Graduate School of Medicine, N-15, W-7, Kita-ku, Sapporo 060-8638, Japan; Phone: +81-11-706-5944; FAX: +81-11-706-5948; email: nodako@med.hokudai.ac.jp

Epithelial-mesenchymal transition (EMT) plays a role in physiologic and pathological conditions, for instance, in embryogenesis, tumor progression, invasion, metastasis, and tissue fibrosis [13]. During EMT, epithelial cells lose their characteristics and acquire the properties of mesenchymal cells. Upon tissue repair-associated events and tissue fibrosis, EMT is known to be triggered by inflammatory cytokines, cytotoxic stress, and DNA damage [13]. Similarly, upon CNV formation retinal pigment epithelial (RPE) cells have been shown to lose their junctional integrity [14] and convert morphologically to fibroblastic-shaped cells [15,16]. These facts led us to the hypothesis that EMT of RPE cells is involved in the fibrotic scar formation in AMD. Indeed, it has been demonstrated that EMT is crucial in the formation of matrix deposition and tissue fibrosis in ocular tissues [17, 18]. Furthermore, inflammatory or angiogenesis-related cytokines, such as VEGF, connective tissue growth factor (CTGF), tumor-necrosis factor (TNF)-α, and transforming growth factor (TGF)–β, which are known to trigger EMT changes, are found in CNV tissues [5,15,19-21]. However, whether and to what extent EMT occurs during the tissue fibrosis of CNV tissue remains unclear.

Table 1. Clinical Information.

Number	Age	Gender	Eye	Visual acuity	Past ocular history
1	64	M	L	20/250	
2	72	M	L	20/200	
3	55	F	R	20/2000	
4	69	M	R	20/100	
5	65	M	R	20/2000	CSC
6	71	M	L	20/300	
7	62	F	R	20/200	CSC
8	73	M	R	20/300	
9	73	F	L	20/50	
10	68	M	R	20/100	CSC
11	69	F	R	15cm/CF	
12	67	M	L	20/500	

CF, counting fingers; CSC, central serous chorioretinopathy.

An important group of transcriptional factors inducing EMT is the Snail family, including Snail (Snail1) and Slug (Snail2), zinc finger proteins that regulate changes in gene-expression patterns. The Snail family suppresses the expression of epithelial molecules like E-Cadherin and zonular occludens (ZO)-1 by binding to the DNA promoter region and stimulating mesenchymal changes, cell mobility, and proliferation in a variety of epithelial cells [22-24]. Furthermore, clinical studies have shown that upregulation of Snail family expression is observed in various tumors originating from epithelial cells [25-28] and in renal fibrosis [29,30], indicating the pivotal role of Snail during EMT. SIP1 (Smad interacting protein 1) is also a zinc finger protein, postulated as an invasion promoter suppressing epithelial adhesion molecule transcription [31]. Snail and SIP1 bind to overlapping promoter sequences and show similar silencing effects [32]. Another molecule known to trigger EMT mechanisms is Twist, a transcription factor containing a helix–loop–helix DNA-binding domain that regulates the Cadherin gene family [33].

The aim of this study is to explore the expression of EMT-associated transcriptional factor(s) in CNV and to determine whether cytokines found in human CNV tissues upregulate the transcription factor(s) for EMT in RPE cells.

METHODS

Specimens: CNV tissues were collected from 12 eyes of 12 patients with AMD (1 eye per patient; 8 males and 4 females, mean age, 67.3±5.2 years old), who underwent pals plana vitrectomy to remove the subfoveal CNV at the Keio University Hospital from 2000 to 2001. The CNV tissues were fixed in 4% PFA immediately after the excision and embedded in paraffin. Serial sections were prepared on glass slides for immunohistochemical staining. Patient records were retrospectively reviewed for clinical characteristics, which are summarized in Table 1. No PDT or intravitreal injection of anti-VEGF agent had been administered in any of the cases before the surgical intervention. The current study was conducted in accordance with the provisions of the Declaration of Helsinki, and written informed consent was obtained before the surgery. The study protocol was approved by the Institutional Review Committee of the Keio University School of Medicine (Tokyo, Japan).

As a control, two postmortem sections of ocular tissues with no retinal diseases (1 section per male from 60- and 62-year-old Caucasian males), obtained from Northwest Lions Eye Bank (Seattle, WA), were used. In addition, normal retinal tissues were obtained from 40-week-old C57Bl/6 mice (n=3; CLEA, Tokyo, Japan), after the animals were sacrificed with an overdose of anesthesia (Ketamine and Xylazine). The animal experiment was conducted in accordance with the ARVO Statement for the Use of Animals in Ophthalmic and Vision Research.

Cell culture: The human RPE cell line ARPE-19 was cultured in a 1:1 mixture of Dulbecco's modified Eagle's medium and Nutrient Mixture F-12 (Invitrogen, Carlsbad, CA), supplemented with 10% (vol/vol) fetal bovine serum (Cambrex, Walkersville, MD), 50 U/ml penicillin, and 50 µg/ml streptomycin on a 35 mm or 60 mm dish (Falcon, Los Angeles, CA). Culture medium was replaced 3 times a week. Cells were maintained at 37 °C, 5% CO_2 in a humidified atmosphere.

Immunohistochemistry and morphometric analysis: Serial paraffin sections were de-paraffinised and rehydrated with a graded series of ethanol. The sections (n=3) were treated for antigen retrieval by pressure boiling in citrate buffer (0.01M, pH 6.0) for 4 min at 121 °C, washed with 0.1% Triton-X, and blocked with 10% normal goat serum (Dako, Carpinteria, CA). Subsequently, the sections were reacted with primary

antibodies at 4 °C overnight: RPE65 (specific marker for RPE: Transduction Laboratories, Lexington, KY) at a dilution of 1:100, α-smooth muscle actin (SMA; Sigma, St. Louis, MO) at a dilution of 1:500, Snail (Abcam, Cambridge, MA) at a dilution of 1:100, Slug (Abcam) at a dilution of 1:250, Twist (Abcam) at a dilution of 1:650, and SIP1 (Abcam) at a dilution of 1:200. After washing, the sections were incubated with Alexa 488 or Alexa 546 conjugated goat anti-rabbit or mouse IgG (Invitrogen) diluted 1:200 in PBS for fluorescent signal detection. The nuclei of cells were counterstained with Hoechst 33258 (Sigma). All antibody concentrations were determined individually by appropriate positive controls. Primary antibodies of the same isotype (Santa Cruz, Santa Cruz, CA) were used as negative control. For morphometric analysis, serial sections (n=3) of CNV were stained by hematoxylin and eosin, and the degree of staining for EMT-associated transcriptional factors and tissue fibrosis was evaluated based on a 4 grade scale: - (negative), + (10% to 40%), ++ (40% to 70%), or +++ (70% to 100%).

ARPE-19 cells were cultured and then were treated with recombinant human TGF-β (10 ng/ml; R&D systems Minneapolis, MN) or VEGF (10 ng/ml; R&D systems) for 8 h. Cells were then fixed with cold methanol/acetone (1:1) for 5 min and permeabilized with 0.1% Triton X-100 for 20 min and were blocked with 10% normal goat serum (Dako, Carpinteria, CA) for 20 min. Cells were incubated with the following primary antibodies at 4 °C overnight: Snail (goat anti-rabbit; Abcam) and N-cadherin (BD Transduction Laboratories, Franklin Lakes, NJ). Cells were then treated with the Alexa 546-conjugated secondary antibody (goat-anti mouse or rabbit, 1:200; Invitrogen) for 60 min. The nuclei of cells were counterstained with Hoechst 33258 (Sigma).

Reverse transcription PCR: ARPE-19 cells were cultured in serum free medium for 24 h and then exposed to TGF-β (10 ng/ml), TNF-α (10 ng/ml; Calbiochem, San Diego, CA), VEGF (10 ng/ml), CTGF (10 ng/ml; Cell Science, Canton, MA), bFGF (10 ng/ml; Invitrogen), and IGF-1 (10 ng/ml; R&D systems) for 4 h at 37 °C. Total RNA was extracted from ARPE-19 cells by the Trizol reagent (Invitrogen) and reverse transcription (RT) was performed using the First-Strand cDNA synthesis kit (GE Healthcare, Buckinghamshire, UK) according to the manufacturer's instructions. PCR products were obtained after 30 cycles of amplification with an annealing temperature of 55 °C using a platinum PCR supermix (Invitrogen). PCR primers were as follows: 5'-AAT CGG AAG CCT AAC TAC AG−3' (forward), 5'- GGA AGA GGC TGA AGT AGA G−3' (reverse) for Snail [34]; 5'- GAA GAG CTA CGA GCT GCC-3' (forward), and 5'- TGA TCC ACA TCT GCT GGA-3' (reverse) for β-actin [35]. PCR products were subjected to electrophoresis on 1.5% agarose gels and visualized by ethidium bromide staining. Quantification of band density was performed using NIH Image 1.41 software (developed by Wayne Rasband, National Institutes of Health, Bethesda, MD). The experiments were performed in duplicate and independently repeated 3 times.

Statistical analyses: All results were expressed as mean±SEM with n-numbers as indicated. Student's *t* test was used for statistical comparison between the groups. Differences were considered statistically significant at $p<0.05$.

RESULTS

Transcriptional factors for EMT in human CNV tissues: To determine whether transcriptional factors for EMT are expressed in retinal tissue under normal conditions, we first stained normal human and mouse retina with antibodies against EMT-associated transcriptional factors. Snail was not detected in the RPE layer of normal retina (Figure 1). Similarly, the other transcriptional factors for EMT, Slug, Twist, and SIP1 were also undetectable in the RPE layer of normal retina (data not shown).

Next we stained for these same factors in surgically excised CNV tissues, tissues composed of blood vessels, stromal cells, and pigmented cells in a fibrous interstitium. The pigmented cells are stained with RPE65, indicating that the cells originated from RPE cells (Figure 2A,B). In CNV tissues, Snail was predominantly detected in the nuclei of the pigmented cells (Figure 2C,D), but it was also found in the nuclei of fibroblast-shaped cells and vascular endothelial cells. Signals for Slug, Twist, and SIP1 were undetectable in the cell nuclei of the CNV tissues (data not shown).

Immunostaining for Snail in the nuclei of RPE65-positive cells was found in 11 of 12 CNV specimens (91.6%, Figure 2 and Table 2). Morphometric analysis showed that CNV tissues with Snail-positive RPE cells (++ or +++) are associated with higher fibrotic changes (++ or +++) in comparison with those containing less Snail-positive RPE cells (Table 2), indicating a relationship between Snail expression and tissue fibrosis in RPE cells. On the cellular level, Snail–positive RPE cells (++ or +++) co-expressed α-SMA (Figure 3, Table 2).

Snail expression in cultured human RPE cells: To explore the cytokines that induce transcription of Snail in RPE cells, we stimulated ARPE-19 cells with candidate cytokines and examined the levels of *Snail* mRNA. First, to determine whether RPE cells constitutively express Snail, we stained ARPE-19 cells with the antibody against Snail. At 2 days after passage, Snail was strongly stained in both the cell nuclei and cytoplasm of cultured RPE cells (Figure 4A). By contrast, after cell-cell contact was established at 7 days after passage, the signal intensity for Snail was reduced in the nuclei and showed faint staining in the cytoplasm compared to those at 2 days after passage (Figure 4B), suggesting that production and cellular localization of Snail in RPE cells is related to the cell density and/or maturation of cell-cell contact.

Next, at 7 days after passage we stimulated ARPE-19 cells with cytokines, TGF-β, TNF-α, VEGF, CTGF, bFGF,

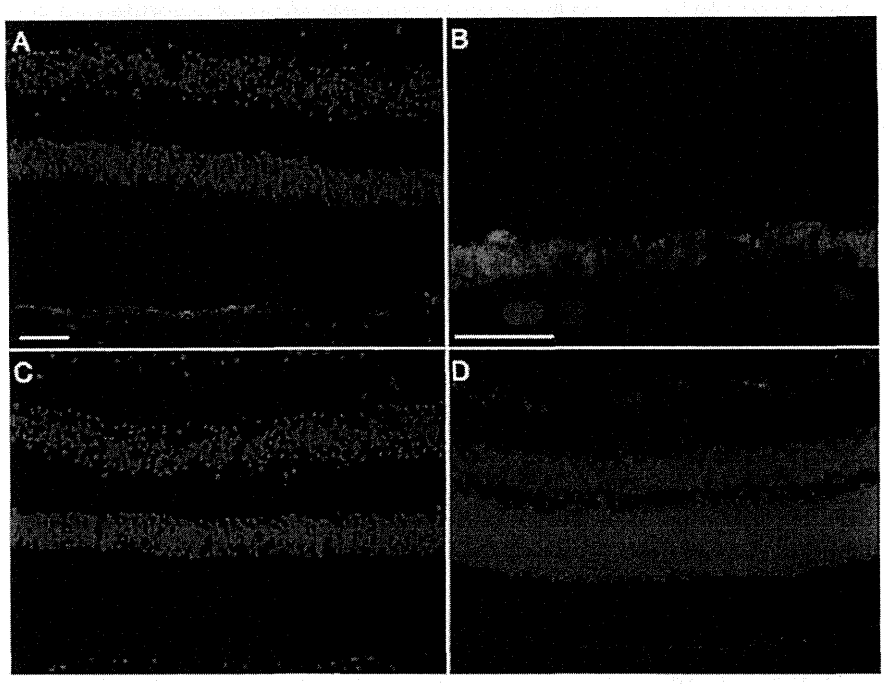

Figure 1. Immunolocalization of Snail protein in normal retina. **A**: Representative immunofluorescent micrograph of Snail (red), RPE65 (green), and nuclear counterstaining with Hoechst 33258 (blue) in normal human retina. **B**: High magnification. **C**: Negative control. **D**: Merged image of a representative immunofluorescent micrograph of Snail (red), RPE65 (green), and nuclear counterstaining with Hoechst 33258 (blue) in normal mouse retina. Scale bars for **A**, **C**, and **D** shown in **A**=50 µm, for **B**=25 µm.

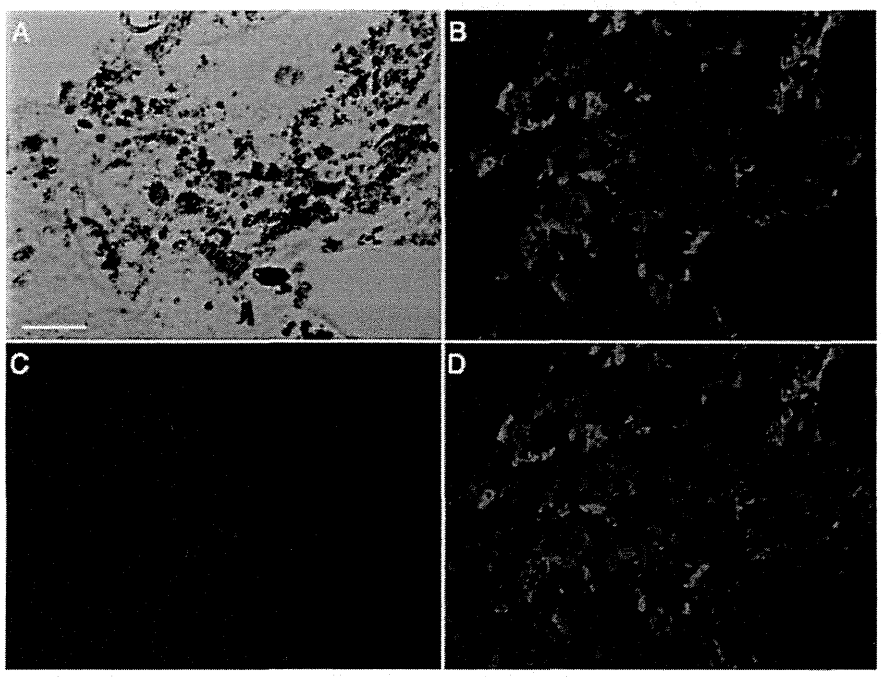

Figure 2. Immunolocalization of Snail protein in human CNV. Representative micrographs of human CNV section. **A**: Phase contrast image. **B**: Fluorescent micrograph of RPE65 (green). **C**: Fluorescent micrograph of Snail (red). **D**: Merged Image. Nuclei were counterstained with Hoechst 33258 (blue). Scale bar=50 µm.

and IGF-1, previously found in human CNV samples. Among them, TGF-β and VEGF significantly upregulated *Snail* mRNA (Figure 5AB). However, the mRNA level of *Snail* was not changed with stimulation of the other cytokines. Furthermore, fluorescence microscopy depicted the enhanced staining of Snail in the nucleus and cytoplasm of ARPE-19 cells stimulated with TGF-β at 7 days after passage (Figure 5C), indicating a role for TGF-β in the upregulation and nuclear relocalization of Snail in RPE cells. By contrast, VEGF enhanced immunoreactivity of Snail mainly in the cytoplasm, but not in the nucleus (Figure 5C).

Snail and N-cadherin in cultured human RPE cells: To study the relationship between Snail and adherence junctions in epithelial integrity, we stained ARPE-19 cells with antibodies

TABLE 2. SNAIL EXPRESSION AND TISSUE FIBROSIS.

Number	Snail-positive RPE	SMA-positive cells	Tissue fibrosis
1	+	+	++
2	++	+	++
3	+++	++	+++
4	+++	++	+++
5	+	++	+
6	-	-	+
7	+	-	+
8	++	+	++
9	++	+	+
10	+++	+++	+++
11	+	-	+
12	++	+	++

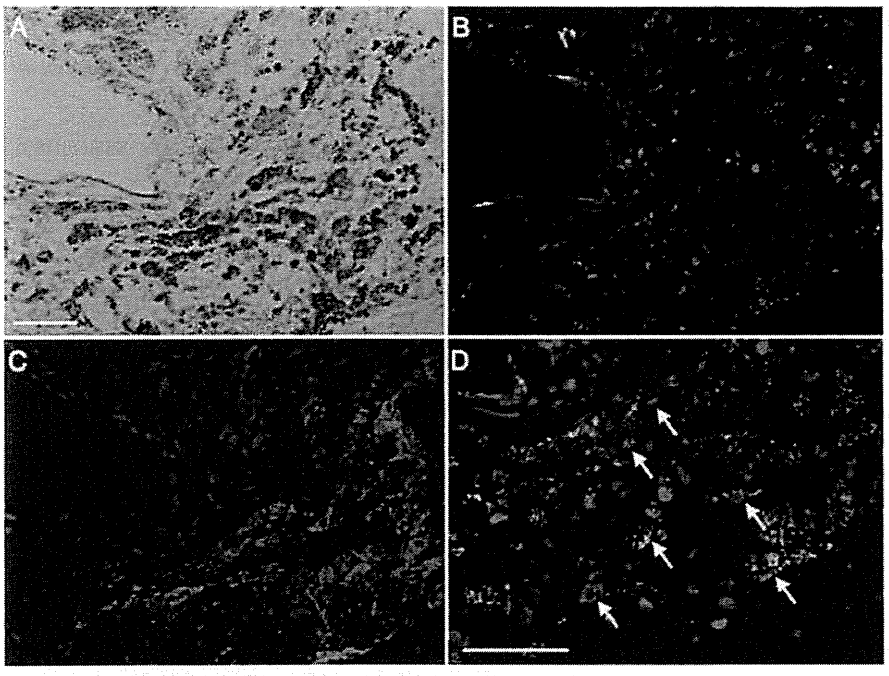

Figure 3. Co-localization of Snail protein and α-SMA in human CNV. Micrographs of a representative section of human CNV. **A**: Phase contrast image. **B**: Fluorescent micrograph of α-SMA (yellow), Snail (red), and cell nuclei (blue). **C**: Consecutive section stained for RPE65 (green), Snail (red), and cell nuclei (blue). **D**: High magnification of **B**. Arrows indicate the co-expression of α-SMA and Snail in RPE cells. Scale bar shown in **A** and **D**=50 μm.

against Snail and N-cadherin before and after establishment of cell-cell contact and with or without TGF-β stimulation. The major cadherin expressed by RPE cells in culture is N-cadherin [36], making N-cadherin a good marker for adherence junction formation in RPE cells.

At 2 days after passage, ARPE-19 showed an increase in Snail expression and a disrupted N-cadherin network (Figure 6A). However, once the cells established the cell-cell contact, N-cadherin expression was markedly upregulated and Snail expression decreased (Figure 6B). Furthermore, TGF-β stimulation caused upregulation of Snail expression and disruption of N-cadherin expression after establishment of cell-cell contact (Figure 6C,D).

DISCUSSION

In the present study, we investigate the expression and localization of EMT-associated transcriptional factors in surgically excised CNV tissues and cultured human RPE cells. The current data indicate that RPE cells migrating into CNV tissues undergo EMT changes mediated by the transcriptional factor, Snail. To our knowledge, this is the first report of the localization of Snail in CNV tissues, a hallmark of wet AMD.

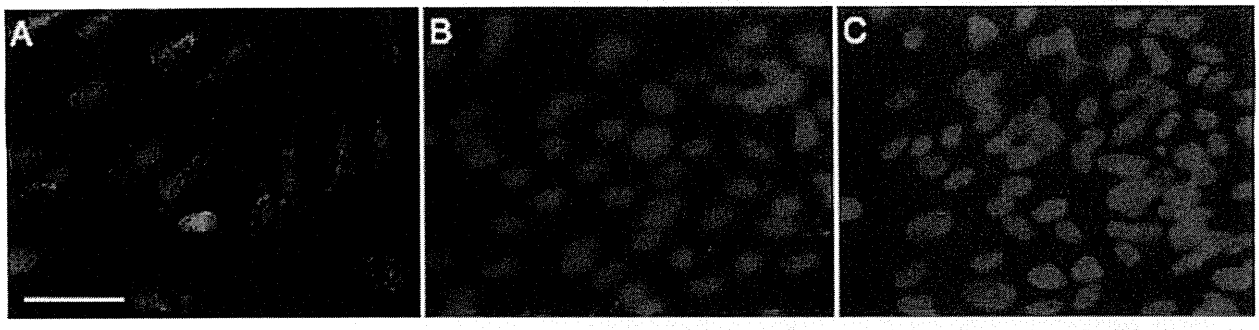

Figure 4. Cellular Localization of Snail in ARPE-19 cells. A: Cellular localization of Snail (red) at 2 days after passage. Snail is observed in both the nuclei and cytoplasm. Nuclei were counterstained with Hoechst 33258 (blue). B: Cellular localization of Snail (red) at 7 days after passage. Snail expression is decreased and observed mainly in the cytoplasm, but not in the nuclei. C: Negative control. Scale bar=50 μm.

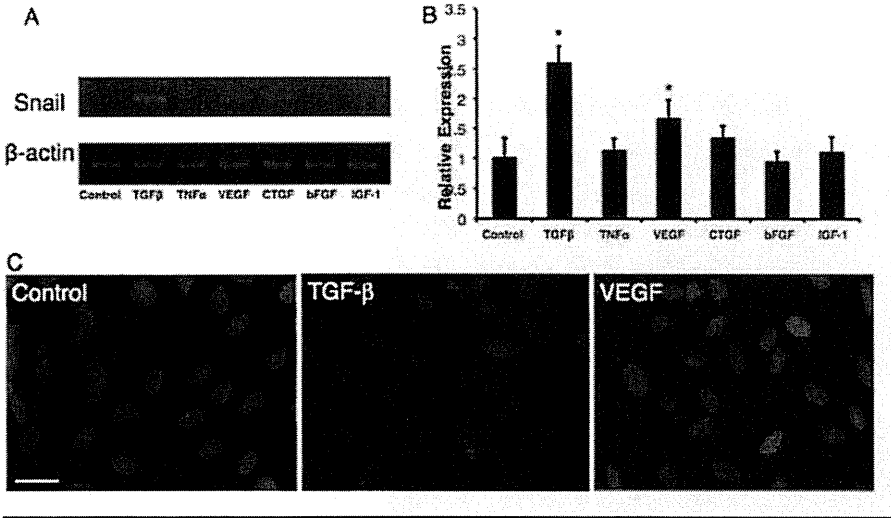

Figure 5. Snail expression after cytokine stimulation in ARPE-19 cells. A: RT–PCR amplification of Snail mRNAs from ARPE-19 cells after cytokine stimulation. ARPE-19 cells were incubated with PBS or recombinant human TGF-β, TNF-α, VEGF, CTGF, bFGF, and IGF-1. After 4 h, RNA was extracted from these cells. Snail mRNA expression was measured by reverse-transcription PCR. B: Gel densitometric analysis. Values are mean±SEM (n=6 in each group). *p<0.05. C: Immunofluorescence for Snail after cytokine stimulation. Left-Control. Middle-8 h after TGF-β stimulation (10 ng/ml). Right-8 h after VEGF stimulation (10 ng/ml). Scale bar=25 μm.

During EMT, epithelial cells lose their polarity and cellular junctions and gain mesenchymal, fibroblast-like morphology and properties [13]. The cellular process is regulated by EMT-associated transcriptional factors such as Snail, Slug, Twist, and SIP1 via suppression of genes encoding adhesion molecules [23]. It has been shown in human tissues that epithelial-derived carcinoma cells and trans-differentiated epithelial cells during tissue fibrosis, both of which have a fibroblast-like morphology, express transcriptional factors relevant to EMT [37,38]. Recently, it has been proposed that EMT can be classified into 3 subtypes, type 1–3 EMTs, based on the biologic context [39]. In brief, type 1 EMTs are associated with implantation and embryo formation. Type 2 EMTs are associated with wound healing, tissue regeneration, and organ fibrosis. The type 2 EMTs begin as part of a repair-associated event that normally generates fibroblasts and other related cells. Type 3 EMTs occur in neoplastic cells that have previously undergone genetic and epigenetic changes. In ocular tissues, the type 2 EMT had been reported to play a role in the pathogenesis of proliferative vitreoretinopathy (PVR) [40,41]. Similar to the proliferative fibrous tissues formed in PVR, CNV tissues contain fibroblasts or cellular constituents with fibroblast-like morphology. In the current study, 92% of the excised CNV tissues showed Snail localization in migrated RPE cells, whereas Slug, Twist, and SIP1 were not detected. By contrast, none of the EMT-associated transcriptional factors was found in normal retinal tissues. Therefore, the current data indicate that Snail is the predominant transcriptional factor mediating EMT (type 2 EMTs) of RPE cells and is induced under the pathological condition of CNV.

Our data show that Snail expression correlates with α-SMA, an established marker for myofibroblasts, and with the amount of tissue fibrosis in CNV tissues. Previously it was reported that choroidal fibroblasts originating from mesenchymal perivascular supporting cells contributed to tissue fibrosis in CNV [42]. In addition to the fibroblasts, the current immunofluorescence study demonstrates that flattened RPE65-positive cells with a fibroblast-like phenotype also express α-SMA with nuclear localization of Snail. CNV tissues in which RPE cells showed higher nuclear localization of Snail positively correlated with the fibrosis

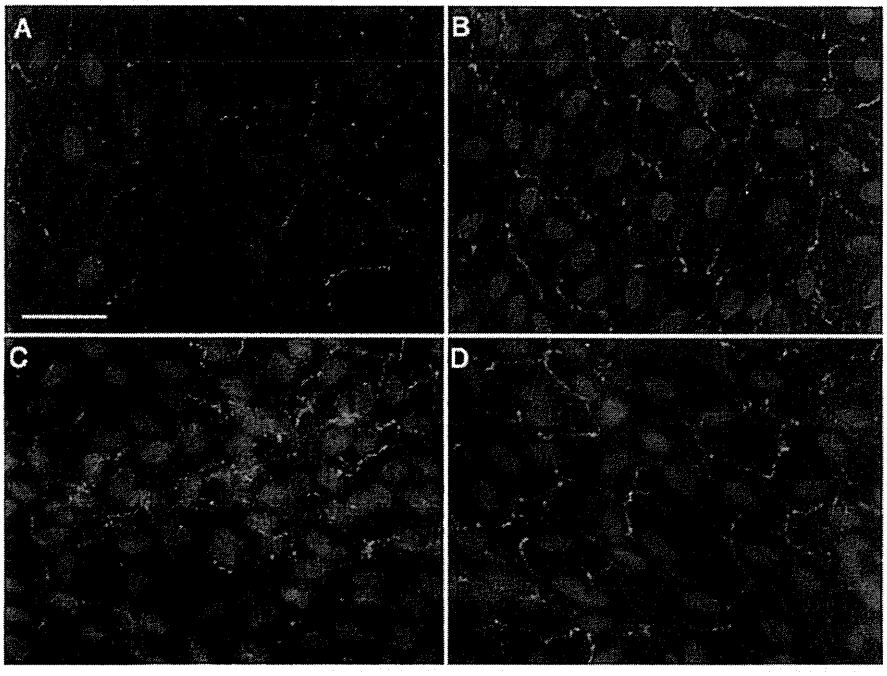

Figure 6. Impact of cell density and TGF-β stimulation on Snail and N-cadherin expression in ARPE-19 cells. **A**: Cellular localization of Snail (red) and N-cadherin (green) at 2 days after passage. Nuclei were counterstained with Hoechst 33258 (blue). **B**: Cellular localization of Snail (red) and N-cadherin (green) at 7 days after passage. **C, D**: Cellular localization of Snail (red) and N-cadherin (green) after **C** TGF-β stimulation (10 ng/ml) and **D** PBS at 7 days after passage. Scale bar=50 µm.

score. Furthermore, the in vitro study showed that cultured RPE cells strongly expressed Snail with disrupted N-cadherin formation before establishing the cell-cell contact, indicating the relevance of Snail to N-cadherin formation in RPE cells. Thus, the current data suggest that the fibroblast-like cells originating, at least in part, from RPE cells undergo type 2 EMTs via the transcriptional factor Snail and contribute to the fibrotic response in the scaring of CNV in concert with fibroblasts [42].

It has been shown that EMT is triggered by cytokine signaling, for instance, TGF-β, VEGF [43], and tumor necrosis factor (TNF)-α [44], which initiate a transcriptional dedifferentiation program correlating with morphological and functional changes [45]. Alternatively, it has also been documented that RPE are transdifferentiated to a mesenchymal phenotype by cytokines, e.g., TGF-β [41] and TNF-α [44]. In accord with previous reports using other cell lines [46,47], the current data demonstrate that Snail expression was upregulated by stimulation of TGF-β and VEGF in cultured human RPE cells. Furthermore, our immunostaining data demonstrate that TGF-β induced nuclear relocalization of Snail and disrupted N-cadherin formation in cultured RPE cells. Since cellular constituents in CNV tissues have been reported to express TGF-β and VEGF [21], the current data suggest that these inflammatory cytokines may induce Snail expression in RPE cells and play a role in the tissue fibrosis of CNV.

In summary, we showed the presence of Snail in human CNV tissues and the role of VEGF and TGF-β in the upregulation and relocalization of Snail in human RPE cells. The data indicate that Snail is a major transcriptional factor for EMT of RPE cells and is involved in the mechanism of scar formation of CNV at the late stage of AMD.

ACKNOWLEDGMENTS

This work was supported by Grant-in-Aid for Young Scientists (B) (05–045–0337) of the Ministry of Education, Culture, Sports, Science and Technology (MEXT), Japan, which provided generous funds for laboratory equipment used in this project. We would like to thank Haruna Koizumi and Ichie Kawamori for their support.

REFERENCES

1. Jager RD, Mieler WF, Miller JW. Age-related macular degeneration. N Engl J Med 2008; 358:2606-17. [PMID: 18550876]
2. Donoso LA, Kim D, Frost A, Callahan A, Hageman G. The role of inflammation in the pathogenesis of age-related macular degeneration. Surv Ophthalmol 2006; 51:137-52. [PMID: 16500214]
3. Green WR. Histopathology of age-related macular degeneration. Mol Vis 1999; 5:27. [PMID: 10562651]
4. Grossniklaus HE, Ling JX, Wallace TM, Dithmar S, Lawson DH, Cohen C, Elner VM, Elner SG, Sternberg P Jr. Macrophage and retinal pigment epithelium expression of angiogenic cytokines in choroidal neovascularization. Mol Vis 2002; 8:119-26. [PMID: 11979237]
5. Schlingemann RO. Role of growth factors and the wound healing response in age-related macular degeneration. Graefes Arch Clin Exp Ophthalmol 2004; 242:91-101. [PMID: 14685874]

6. Winkler BS, Boulton ME, Gottsch JD, Sternberg P. Oxidative damage and age-related macular degeneration. Mol Vis 1999; 5:32. [PMID: 10562656]
7. Zarbin MA. Current concepts in the pathogenesis of age-related macular degeneration. Arch Ophthalmol 2004; 122:598-614. [PMID: 15078679]
8. Wormald R, Evans J, Smeeth L, Henshaw K. Photodynamic therapy for neovascular age-related macular degeneration. Cochrane Database Syst Rev 2005; (4):CD002030. [PMID: 16235294]
9. Ip MS, Scott IU, Brown GC, Brown MM, Ho AC, Huang SS, Recchia FM. Anti-vascular endothelial growth factor pharmacotherapy for age-related macular degeneration: a report by the American Academy of Ophthalmology. Ophthalmology 2008; 115:1837-46. [PMID: 18929163]
10. Kumar A, Gopalakrishnan K, Sinha S. Combination photodynamic therapy and intravitreal ranibizumab in neovascular AMD in a north Indian population: a pilot study. Retina 2008; 28:1132-7. [PMID: 18779720]
11. Smith BT, Dhalla MS, Shah GK, Blinder KJ, Ryan EH Jr, Mittra RA. Intravitreal injection of bevacizumab combined with verteporfin photodynamic therapy for choroidal neovascularization in age-related macular degeneration. Retina 2008; 28:675-81. [PMID: 18463509]
12. Riusala A, Sarna S, Immonen I. Visual acuity and structural findings in old age-related macular degeneration. Graefes Arch Clin Exp Ophthalmol 2005; 243:947-50. [PMID: 15834599]
13. Thiery JP, Sleeman JP. Complex networks orchestrate epithelial-mesenchymal transitions. Nat Rev Mol Cell Biol 2006; 7:131-42. [PMID: 16493418]
14. Bailey TA, Kanuga N, Romero IA, Greenwood J, Luthert PJ, Cheetham ME. Oxidative stress affects the junctional integrity of retinal pigment epithelial cells. Invest Ophthalmol Vis Sci 2004; 45:675-84. [PMID: 14744914]
15. Lopez PF, Sippy BD, Lambert HM, Thach AB, Hinton DR. Transdifferentiated retinal pigment epithelial cells are immunoreactive for vascular endothelial growth factor in surgically excised age-related macular degeneration-related choroidal neovascular membranes. Invest Ophthalmol Vis Sci 1996; 37:855-68. [PMID: 8603870]
16. Watanabe D, Takagi H, Suzuma K, Oh H, Ohashi H, Honda Y. Expression of connective tissue growth factor and its potential role in choroidal neovascularization. Retina 2005; 25:911-8. [PMID: 16205572]
17. Saika S, Kono-Saika S, Tanaka T, Yamanaka O, Ohnishi Y, Sato M, Muragaki Y, Ooshima A, Yoo J, Flanders KC, Roberts AB. Smad3 is required for dedifferentiation of retinal pigment epithelium following retinal detachment in mice. Lab Invest 2004; 84:1245-58. [PMID: 15273699]
18. Saika S, Yamanaka O, Flanders KC, Okada Y, Miyamoto T, Sumioka T, Shirai K, Kitano A, Miyazaki K, Tanaka S, Ikeda K. Epithelial-mesenchymal transition as a therapeutic target for prevention of ocular tissue fibrosis. Endocr Metab Immune Disord Drug Targets 2008; 8:69-76. [PMID: 18393925]
19. Amin R, Puklin JE, Frank RN. Growth factor localization in choroidal neovascular membranes of age-related macular degeneration. Invest Ophthalmol Vis Sci 1994; 35:3178-88. [PMID: 7519180]
20. He S, Jin ML, Worpel V, Hinton DR. A role for connective tissue growth factor in the pathogenesis of choroidal neovascularization. Arch Ophthalmol 2003; 121:1283-8. [PMID: 12963611]
21. Oh H, Takagi H, Takagi C, Suzuma K, Otani A, Ishida K, Matsumura M, Ogura Y, Honda Y. The potential angiogenic role of macrophages in the formation of choroidal neovascular membranes. Invest Ophthalmol Vis Sci 1999; 40:1891-8. [PMID: 10440240]
22. Barrallo-Gimeno A, Nieto MA. The Snail genes as inducers of cell movement and survival: implications in development and cancer. Development 2005; 132:3151-61. [PMID: 15983400]
23. Katoh M, Katoh M. Comparative genomics on SNAI1, SNAI2, and SNAI3 orthologs. Oncol Rep 2005; 14:1083-6. [PMID: 16142376]
24. Nieto MA, Bennett MF, Sargent MG, Wilkinson DG. Cloning and developmental expression of Sna, a murine homologue of the Drosophila snail gene. Development 1992; 116:227-37. [PMID: 1483390]
25. Blanco MJ, Moreno-Bueno G, Sarrio D, Locascio A, Cano A, Palacios J, Nieto MA. Correlation of Snail expression with histological grade and lymph node status in breast carcinomas. Oncogene 2002; 21:3241-6. [PMID: 12082640]
26. Jiao W, Miyazaki K, Kitajima Y. Inverse correlation between E-cadherin and Snail expression in hepatocellular carcinoma cell lines in vitro and in vivo. Br J Cancer 2002; 86:98-101. [PMID: 11857019]
27. Rosivatz E, Becker I, Specht K, Fricke E, Luber B, Busch R, Hofler H, Becker KF. Differential expression of the epithelial-mesenchymal transition regulators snail, SIP1, and twist in gastric cancer. Am J Pathol 2002; 161:1881-91. [PMID: 12414534]
28. Waldmann J, Feldmann G, Slater EP, Langer P, Buchholz M, Ramaswamy A, Saeger W, Rothmund M, Fendrich V. Expression of the zinc-finger transcription factor Snail in adrenocortical carcinoma is associated with decreased survival. Br J Cancer 2008; 99:1900-7. [PMID: 19018264]
29. Boutet A, De Frutos CA, Maxwell PH, Mayol MJ, Romero J, Nieto MA. Snail activation disrupts tissue homeostasis and induces fibrosis in the adult kidney. EMBO J 2006; 25:5603-13. [PMID: 17093497]
30. Boutet A, Esteban MA, Maxwell PH, Nieto MA. Reactivation of Snail genes in renal fibrosis and carcinomas: a process of reversed embryogenesis? Cell Cycle 2007; 6:638-42. [PMID: 17374993]
31. Comijn J, Berx G, Vermassen P, Verschueren K, van Grunsven L, Bruyneel E, Mareel M, Huylebroeck D, van Roy F. The two-handed E box binding zinc finger protein SIP1 downregulates E-cadherin and induces invasion. Mol Cell 2001; 7:1267-78. [PMID: 11430829]
32. Burke JM. Epithelial phenotype and the RPE: is the answer blowing in the Wnt? Prog Retin Eye Res 2008; 27:579-95. [PMID: 18775790]
33. Oda H, Tsukita S, Takeichi M. Dynamic behavior of the cadherin-based cell-cell adhesion system during Drosophila gastrulation. Dev Biol 1998; 203:435-50. [PMID: 9808792]
34. Espineda CE, Chang JH, Twiss J, Rajasekaran SA, Rajasekaran AK. Repression of Na,K-ATPase beta1-subunit by the transcription factor snail in carcinoma. Mol Biol Cell 2004; 15:1364-73. [PMID: 14699059]

35. Liu XH, Kirschenbaum A, Lu M, Yao S, Dosoretz A, Holland JF, Levine AC. Prostaglandin E2 induces hypoxia-inducible factor-1alpha stabilization and nuclear localization in a human prostate cancer cell line. J Biol Chem 2002; 277:50081-6. [PMID: 12401798]
36. Van Aken EH, De Wever O, Van Hoorde L, Bruyneel E, De Laey JJ, Mareel MM. Invasion of retinal pigment epithelial cells: N-cadherin, hepatocyte growth factor, and focal adhesion kinase. Invest Ophthalmol Vis Sci 2003; 44:463-72. [PMID: 12556370]
37. Elloul S, Elstrand MB, Nesland JM, Trope CG, Kvalheim G, Goldberg I, Reich R, Davidson B. Snail, Slug, and Smad-interacting protein 1 as novel parameters of disease aggressiveness in metastatic ovarian and breast carcinoma. Cancer 2005; 103:1631-43. [PMID: 15742334]
38. Kojc N, Zidar N, Gale N, Poljak M, Fujs Komlos K, Cardesa A, Hofler H, Becker KF. Transcription factors Snail, Slug, Twist, and SIP1 in spindle cell carcinoma of the head and neck. Virchows Arch 2009; 454:549-55. [PMID: 19381684]
39. Kalluri R, Weinberg RA. The basics of epithelial-mesenchymal transition. J Clin Invest 2009; 119:1420-8. [PMID: 19487818]
40. Grisanti S, Guidry C. Transdifferentiation of retinal pigment epithelial cells from epithelial to mesenchymal phenotype. Invest Ophthalmol Vis Sci 1995; 36:391-405. [PMID: 7531185]
41. Parapuram SK, Chang B, Li L, Hartung RA, Chalam KV, Nair-Menon JU, Hunt DM, Hunt RC. Differential effects of TGFbeta and vitreous on the transformation of retinal pigment epithelial cells. Invest Ophthalmol Vis Sci 2009; 50:5965-74. [PMID: 19578024]
42. Kent D, Sheridan C. Choroidal neovascularization: a wound healing perspective. Mol Vis 2003; 9:747-55. [PMID: 14735062]
43. Gonzalez-Moreno O, Lecanda J, Green JE, Segura V, Catena R, Serrano D, Calvo A. VEGF elicits epithelial-mesenchymal transition (EMT) in prostate intraepithelial neoplasia (PIN)-like cells via an autocrine loop. Exp Cell Res 2010; 316:554-67. [PMID: 20006606]
44. Takahashi E, Nagano O, Ishimoto T, Yae T, Suzuki Y, Shinoda T, Nakamura S, Niwa S, Ikeda S, Koga H, Tanihara H, Saya H. Tumor necrosis factor-alpha regulates transforming growth factor-beta-dependent epithelial-mesenchymal transition by promoting hyaluronan-CD44-moesin interaction. J Biol Chem 2010; 285:4060-73. [PMID: 19965872]
45. Vetter G, Le Bechec A, Muller J, Muller A, Moes M, Yatskou M, Al Tanoury Z, Poch O, Vallar L, Friederich E. Time-resolved analysis of transcriptional events during SNAI1-triggered epithelial to mesenchymal transition. Biochem Biophys Res Commun 2009; 385:485-91. [PMID: 19442650]
46. Peinado H, Quintanilla M, Cano A. Transforming growth factor beta-1 induces snail transcription factor in epithelial cell lines: mechanisms for epithelial mesenchymal transitions. J Biol Chem 2003; 278:21113-23. [PMID: 12665527]
47. Wanami LS, Chen HY, Peiro S, Garcia de Herreros A, Bachelder RE. Vascular endothelial growth factor-A stimulates Snail expression in breast tumor cells: implications for tumor progression. Exp Cell Res 2008; 314:2448-53. [PMID: 18554584]

Articles are provided courtesy of Emory University and the Zhongshan Ophthalmic Center, Sun Yat-sen University, P.R. China. The print version of this article was created on 3 May 2011. This reflects all typographical corrections and errata to the article through that date. Details of any changes may be found in the online version of the article.

Case Reports in Ophthalmology

Case Rep Ophthalmol 2011;2:307–313
DOI: 10.1159/000332734

Published online: September 19, 2011

ISSN 1663–2699
www.karger.com/cop

Focal Functional and Microstructural Changes of Photoreceptors in Eyes with Acute Zonal Occult Outer Retinopathy

Keitetsu So[a] Kei Shinoda[a] Celso Soiti Matsumoto[a]
Shingo Satofuka[a] Yutaka Imamura[b] Atsushi Mizota[a, c]

[a]Department of Ophthalmology, Teikyo University School of Medicine, University Hospital Itabashi, Tokyo, [b]Department of Ophthalmology, Teikyo University School of Medicine, University Hospital Mizonokuchi, Kawasaki, and [c]Department of Ophthalmology, Juntendo University Urayasu Hospital, Chiba, Japan

Key Words
Acute zonal occult outer retinopathy · Perimetry · Multifocal electroretinogram · Optical coherence tomography · External limiting membrane · Photoreceptor inner and outer segment line · IS/OS line · Cone outer segment tips

Abstract
Purpose: Acute zonal occult outer retinopathy (AZOOR) is characterized by an acute zonal loss of outer retinal function with minimal ophthalmoscopic changes in one or both eyes. We present a patient with AZOOR whose ultrastructural and functional findings were followed for 8 months.
Case: A 22-year-old woman developed an acute central scotoma in her right eye. Her best-corrected visual acuity (BCVA) was 0.5 OD and 1.2 OS. The ophthalmoscopic examinations, fluorescein angiography, and full-field electroretinograms (ERGs) were normal in both eyes. The amplitudes of the multifocal ERGs (mfERGs) were attenuated in the area corresponding to the scotoma. Spectral domain optical coherence tomography showed an absence of both the inner and outer segment (IS/OS) line of the photoreceptors and the cone outer segment tip (COST) line between the IS/OS line and the retinal pigment epithelium. These changes were seen in the area corresponding to the scotoma. One month later, the scotoma disappeared and the BCVA improved to 1.2 OD. The mfERGs increased to almost the same amplitude as the fellow eye. The IS/OS line became discernible but the COST line was still absent. The ophthalmological findings of the right macula remained normal during the 11-month follow-up period.

Kei Shinoda, MD
Department of Ophthalmology, Teikyo University School of Medicine
2-11-1 Kaga, Itabashi-ku, Tokyo 173-8605 (Japan)
Tel. +81 3 3964 1225, E-Mail shinodak@med.teikyo-u.ac.jp

Case Reports in Ophthalmology
Case Rep Ophthalmol 2011;2:307–313
DOI: 10.1159/000332734
Published online: September 19, 2011

ISSN 1663–2699
www.karger.com/cop

Conclusions: Our findings indicate that the selective loss of the IS/OS and the COST lines is probably the morphological alterations corresponding with the reduced BCVA and the mfERGs in the areas of the visual field defects in the acute phase of AZOOR. But in the recovery phase, only the abnormality of the COST line is a subclinical sign for the disease. These findings should be important in understanding and evaluating the pathological mechanism in other outer retinal diseases.

Introduction

Acute zonal occult outer retinopathy (AZOOR) is a uni- or bilateral disease characterized by an acute zonal loss of outer retinal function with minimal ophthalmoscopic changes [1]. It is associated with other clinical diseases including acute idiopathic blind spot enlargement syndrome, acute macular neuroretinopathy, multiple evanescent white dot syndrome, multifocal choroiditis, and panuveitis. These are all believed to have a similar etiology and are called the AZOOR complex [1–4].

Optical coherence tomography (OCT) of eyes with the AZOOR complex showed abnormalities in the microstructures of the outer retina, e.g., disruption or loss of the external limiting membrane (ELM), the inner and outer segment (IS/OS) line, or the cone outer segment tip (COST) line [5]. The COST line is a thin highly reflective line located between the IS/OS junction and the retinal pigment epithelium (RPE), and it is absent in the areas where the visual field defects are present [4, 6–11]. However, the pathophysiological interpretation of the intactness of this line, and the diagnostic value of the COST line have not been established.

We have examined a patient with AZOOR and followed the changes in the ultrastructure and function in the area of the focal retinal lesion.

Case Report

A 22-year-old Japanese woman complained of a central scotoma in the right eye. Her best-corrected visual acuity (BCVA) was 0.5 with a correction of –4.0 diopter in the right eye and 1.2 with –4.5 diopter in the left eye. The intraocular pressure was 14 mm Hg OU. The anterior segment was normal. Ophthalmoscopy and fluorescein angiography (FA) showed that the retina and choroid were normal. Humphrey perimetry tested with central 30-2 program and SITA-Fast strategy (Humphrey Field Analyzer, Carl Zeiss, San Leandro, Calif., USA) for central 30 degree demonstrated a relative central scotoma in the right eye (fig. 1). Single flash, full-field mixed rod and cone electroretinograms (ERGs), photopic cone ERGs, and oscillatory potentials were recorded according to ISCEV standard for ERG [12] using LED built-in contact lens electrode (EW-102, Mayo, Inazawa, Japan). All responses were normal in both eyes. The multifocal ERGs (mfERGs) were recorded with a VERIS recording system (EDI, San Mateo, Calif., USA). The visual stimulus consisted of 61 hexagonal elements scaled in size to give approximately equal-amplitude local responses with eccentricity. The amplitudes of the mfERGs were reduced in the area corresponding to the visual field defects in the right eye (fig. 1).

The entire macular area was scanned with a spectral domain optical coherence tomography (SD-OCT) instrument (Cirrus OCT; Carl Zeiss Meditec, Inc.) with scan lengths of 9 mm. High quality images were obtained by using the 5-line raster mode. The ELM was distinct in the SD-OCT images, whereas the IS/OS lines and the COST line between the IS/OS and RPE in the macula of the right eye were not detected (fig. 1). These ophthalmological findings and negative serological findings were compatible with AZOOR, and no special treatment was used.

Case Rep Ophthalmol 2011;2:307–313
DOI: 10.1159/000332734
Published online: September 19, 2011

ISSN 1663–2699
www.karger.com/cop

One month later, the central scotoma disappeared and repeated Humphrey perimetry detected no abnormality anymore. The visual acuity improved to 1.2 in the right eye. The amplitudes of the mfERGs recovered to the same level as that of the healthy fellow eye (fig. 2). The IS/OS line became discernible but the COST line was still absent (fig. 2). These ophthalmological findings, except the ultrastructure of the right macula, remain normal during the 11-month follow-up examinations.

Discussion

Several authors have suggested that the primary site of the pathology in the AZOOR complex is the photoreceptors [1–4, 9]. In support of this, the time domain OCT images showed that the IS/OS line was irregular and indistinct in a patient with AZOOR, and the authors suggested that the pathology was in the photoreceptor outer segments [6].

Recent improvements in the resolution of OCT have allowed better evaluations of the intraretinal microstructures in several retinal diseases [13]. The OCT images showed that the presence of a continuous IS/OS line was due to well-restored photoreceptor cells [5], and the integrity of the ELM was correlated with the morphologic changes in the photoreceptor cell bodies and Müller cells [14, 15]. Srinivasan et al. [5] reported that the highly reflective line between the IS/OS junction and the RPE was the COST line, and it was visible because of the different lengths of the cone and rod OSs. A correlation was found between the site of the visual impairments and the loss of the foveal COST line in several retinal diseases including macular hole, occult macular dystrophy, and the AZOOR complex [11, 16, 17]. All of these reports focused on the microstructure and reported that the integrity of the microstructure was correlated with the BCVA, i.e., absence of IS/OS, ELM, and/or COSTs was present in eyes with decreased BCVA and their intactness coexisted with good BCVA. In addition, a significant correlation was present between these morphological changes and the BCVA.

Our findings showed a discrepancy between the microstructural findings and the visual functions, i.e., good BCVA, normal visual fields, and normal-size mfERGs in spite of an absence of the COST line. To the best of our knowledge, our findings are the first to compare the microstructure of the photoreceptors and visual function in the course of AZOOR.

Kondo et al. [18] reported that the attenuated mfERGs remained even after the visual acuity and visual field had only partially recovered to normal levels in a patient with acute idiopathic blind spot enlargement syndrome. They attributed the discrepancy between perimetry and the mfERGs to methodological differences, i.e., the mfERGs are elicited by suprathreshold stimulus intensities from localized regions, whereas static perimetry employs near threshold stimuli. The mfERGs sum the activity of sensitive and insensitive cells from the stimulated retina, whereas the psychophysical threshold is determined by the activity of the most sensitive cells [19].

In our case, an absence of the COST line was observed even after recovery of the cone function detected by perimetry and mfERGs. These findings suggest that the COST line is the most sensitive parameter for the pathology of the retina. Alternatively, the absence of the COST line does not necessarily mean a clinically discernible dysfunction of the central cone photoreceptors once the disease develops. What the absence of the COST line means and whether it will recover in this case are unknown. Further longitudinal studies on a

Case Rep Ophthalmol 2011;2:307–313
DOI: 10.1159/000332734
Published online: September 19, 2011

ISSN 1663–2699
www.karger.com/cop

large number of patients are required to determine the underlying pathology and the meaning of the integrity of the photoreceptor microstructure detected by SD-OCT.

Our findings were made on a single case of AZOOR, and they cannot be extended to all cases of AZOOR until further studies are done. But observations of the integrity of outer retinal microstructure including the ELM, IS/OS line, and the COST line in correlation with functional parameters would be informative and clinically relevant to the understanding of the pathologic mechanism and to the determination of the severity or stage of different retinal diseases.

Acknowledgement

Support of this study was provided by Research Grants on Sensory and Communicative Disorders from the Ministry of Health, Labor, and Welfare, Japan.

Disclosure Statement

No author has a financial or proprietary interest in any material or method mentioned.

Case Rep Ophthalmol 2011;2:307–313
DOI: 10.1159/000332734
Published online: September 19, 2011

ISSN 1663–2699
www.karger.com/cop

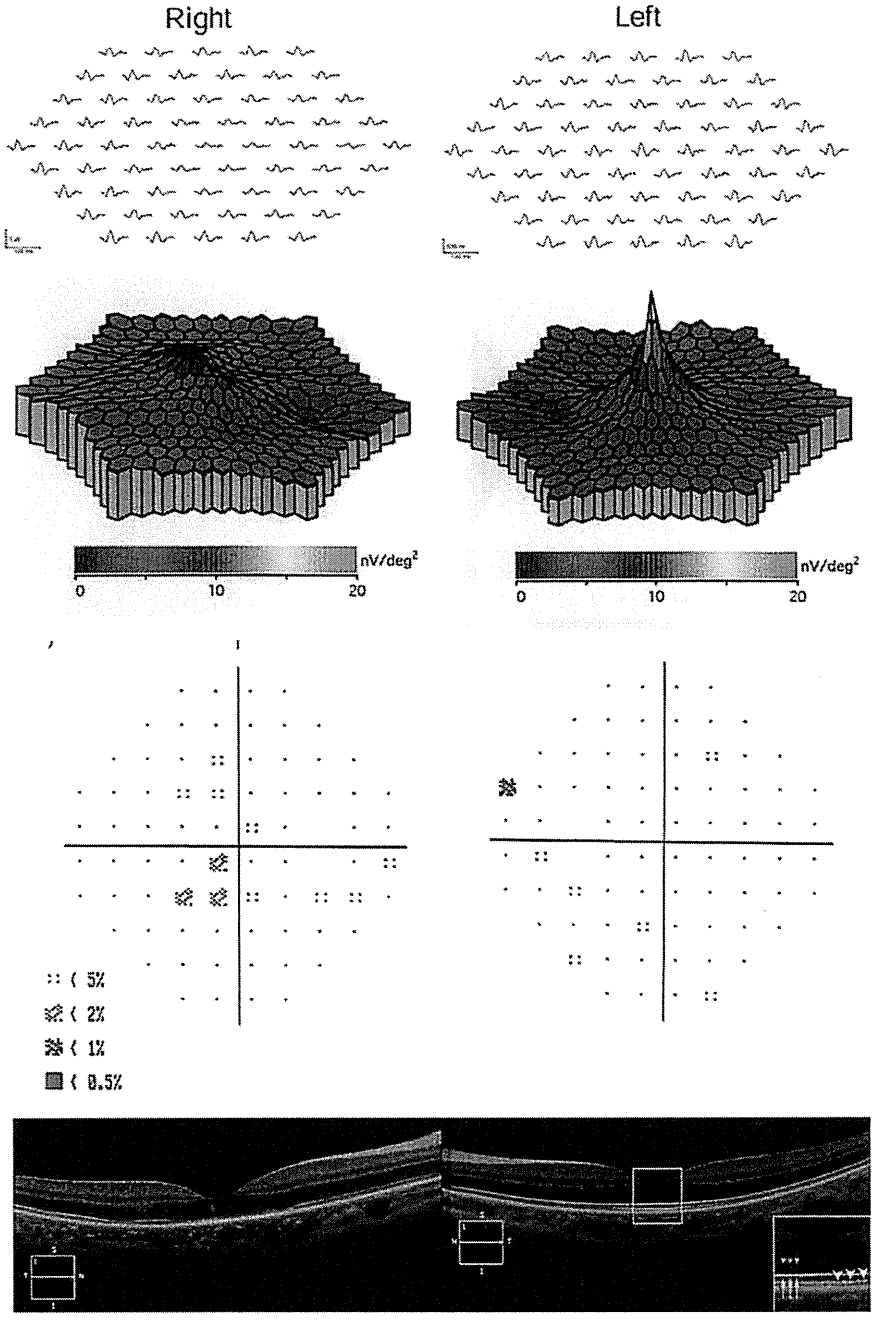

Fig. 1. Clinical findings of a patient at the acute phase of AZOOR. The visual acuity was 0.5 OD and 1.2 OS. First and second rows: mfERGs of the 61 response arrays and 3-dimensional plot of the mfERGs, respectively. These mfERGs show the reduced responses in the area corresponding with the visual field defect. The third row shows the pattern deviation probability map of the Humphrey static visual field tested with central 30-2 program and SITA-Fast strategy (Humphrey Field Analyzer, Carl Zeiss, San Leandro, Calif., USA) for central 30 degree. The mean deviation was –1.04 dB in the right eye and –2.25 dB in the left eye, and the probability map shows a reduced sensitivity in the central area of the right eye. The bottom row shows the Fourier-domain optical coherence tomographic images from the affected right eye and normal left eye. These images show that both the photoreceptor IS/OS line and the COST line between the IS/OS line and RPE are absent in the macula area of the right eye. The IS/OS line, COST line, and the RPE/Bruch membrane are intact in the left eye. Arrowheads indicate ELM. Arrows indicate IS/OS. Large arrowheads indicate COST line.

Case Rep Ophthalmol 2011;2:307–313
DOI: 10.1159/000332734
Published online: September 19, 2011

ISSN 1663–2699
www.karger.com/cop

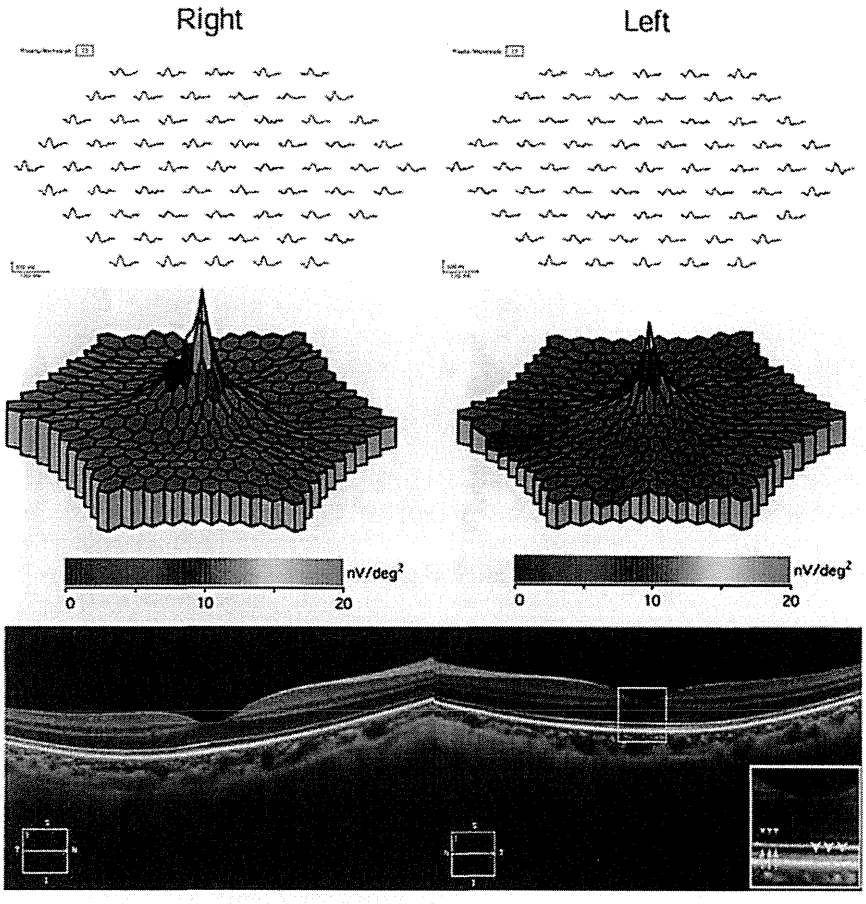

Fig. 2. Clinical findings of our AZOOR patient at the recovery phase. Visual acuity was 1.2 OU. The top and the second row panels are 61 response arrays and 3-dimensional plot of the multifocal electroretinograms, respectively. These show a recovery of the functions in the central area of the right eye. The bottom panels are Fourier-domain optical coherence tomographic images from both eyes, showing that the border of the photoreceptor IS/OS line is clearly discernible but the COST line is still absent in the foveal area of the right eye. The IS/OS line, COST line, and the RPE/Bruch membrane are intact in the left eye. Arrowheads indicate ELM. Arrows indicate IS/OS. Large arrowheads indicate COST line.

References

1 Gass JD: Acute zonal occult outer retinopathy. Donders Lecture: The Netherlands Ophthalmological Society, Maastricht, Holland, June 19, 1992. J Clin Neuroophthalmol 1993;13:79–97.

2 Gass JD, Agarwal A, Scott IU: Acute zonal occult outer retinopathy: a long-term follow-up study. Am J Ophthalmol 2002;134:329–339.

3 Gass JD: Are acute zonal occult outer retinopathy and the white spot syndromes (AZOOR complex) specific autoimmune diseases? Am J Ophthalmol 2003;135:380–381.

4 Spaide RF, Koizumi H, Freund KB: Photoreceptor outer segment abnormalities as a cause of blind spot enlargement in acute zonal occult outer retinopathy-complex diseases. Am J Ophthalmol 2008;146:111–120.

5 Srinivasan VJ, Monson BK, Wojtkowski M, et al: Characterization of outer retinal morphology with high-speed, ultrahigh-resolution optical coherence tomography. Invest Ophthalmol Vis Sci 2008;49:1571–1579.

6 Li D, Kishi S: Loss of photoreceptor outer segment in acute zonal occult outer retinopathy. Arch Ophthalmol 2007;125:1194–1200.

Case Rep Ophthalmol 2011;2:307–313
DOI: 10.1159/000332734
Published online: September 19, 2011

ISSN 1663–2699
www.karger.com/cop

7 Takai Y, Ishiko S, Kagokawa H, Fukui K, Takahashi A, Yoshida A: Morphological study of acute zonal occult outer retinopathy (AZOOR) by multiplanar optical coherence tomography. Acta Ophthalmol 2009;87:408–418.

8 Zibrandtsen N, Munch IC, Klemp K, Jørgensen TM, Sander B, Larsen M: Photoreceptor atrophy in acute zonal occult outer retinopathy. Acta Ophthalmol 2008;86:913–916.

9 Fujiwara T, Imamura Y, Giovinazzo VJ, Spaide RF: Fundus autofluorescence and optical coherence tomographic findings in acute zonal occult outer retinopathy. Retina 2010;30:1206–1216.

10 Ohta K, Sato A, Fukui E: Spectral domain optical coherence tomographic findings at convalescent stage of acute zonal occult outer retinopathy. Clin Ophthalmol 2009;3:423–428.

11 Sugahara M, Shinoda K, Matsumoto CS, Satofuka S, Hanazono G, Imamura Y, Mizota A: Outer retinal microstructure in case of acute idiopathic blind spot enlargement syndrome. Case Rep Ophthalmol 2011;2:116–122.

12 Marmor MF, Fulton AB, Holder GE, Miyake Y, Brigell M, Bach M: Standard for clinical electroretinography (2008 update). Doc Ophthalmol 2009;118:69–77.

13 Byeon SH, Kang SY: Interpretation of outer retina appearance in high-resolution optical coherence tomography. Am J Ophthalmol 2009;147:185–186.

14 Lim JI, Tan O, Fawzi AA, Hopkins JJ, Gil-Flamer JH, Huang D: A pilot study of Fourier-domain optical coherence tomography of retinal dystrophy patients. Am J Ophthalmol 2008;146:417–426.

15 Wakabayashi T, Oshima Y, Fujimoto H, Murakami Y, Sakaguchi H, Kusaka S, Tano Y: Foveal microstructure and visual acuity after retinal detachment repair. Ophthalmology 2009;116:519–528.

16 Wakabayashi T, Fujiwara M, Sakaguchi H, Kusaka S, Oshima Y: Foveal microstructure and visual acuity in surgically closed macular holes: spectral-domain optical coherence tomographic analysis. Ophthalmology 2010;117:1815–1824.

17 Park SJ, Woo SJ, Park KH, Hwang JM, Chung H: Morphologic photoreceptor abnormality in occult macular dystrophy on spectral-domain optical coherence tomography. Invest Ophthalmol Vis Sci 2010;51:3673–3679.

18 Kondo N, Kondo M, Miyake Y: Acute idiopathic blind spot enlargement syndrome: prolonged retinal dysfunction revealed by multifocal electroretinogram technique. Am J Ophthalmol 2001;132:126–128.

19 Hood DC, Zhang X: Multifocal ERG and VEP responses and visual fields: comparing disease-related changes. Doc Ophthalmol 2000;100:115–137.

1040-5488/12/8905-0684/0 VOL. 89, NO. 5, PP. 684–691
OPTOMETRY AND VISION SCIENCE

ORIGINAL ARTICLE

Autosomal Dominant Occult Macular Dystrophy with an *RP1L1* Mutation (R45W)

Takaaki Hayashi*, Tamaki Gekka*, Kenichi Kozaki*, Yasuhiro Ohkuma†, Isako Tanaka*, Hisashi Yamada*, and Hiroshi Tsuneoka*

ABSTRACT

Purpose. To characterize clinical features in occult macular dystrophy (OMD) patients with the *RP1L1* gene mutation (p.R45W), one of two previously described mutations in Japanese OMD patients.

Methods. Mutational screening of the *RP1L1* gene was performed via polymerase chain reaction and direct sequencing for seven unrelated probands (one autosomal dominant and six sporadic probands) with OMD. A comprehensive ophthalmic examination was performed, including Cirrus optical coherence tomography. Full-field electroretinography (ERG), multifocal ERG, and focal macular ERG were performed.

Results. The heterozygous mutation (p.R45W) was found in only one female proband with autosomal dominant OMD, whose mother was also diagnosed with OMD and carried the mutation. Ophthalmoscopy showed bilateral normal fundi in the proband but subtle retinal pigment epithelium mottling in the mother. Both the proband and her mother had typical OMD findings: decreased visual acuity and markedly reduced central responses in the multifocal ERG and focal macular ERG. Although full-field ERG revealed normal rod and standard combined responses, photopic and 30-Hz flicker responses were slightly reduced in both the proband and her mother. Optical coherence tomography revealed that the external limiting membrane and inner segment-outer segment boundary were disorganized despite normal macular thickness in the proband, whereas the mother exhibited macular thinning with discontinuous reflectivity of the external limiting membrane and inner segment-outer segment boundary.

Conclusions. The clinical phenotypes differed between the proband and her mother and were indistinguishable from other sporadic or *RP1L1*-unassociated OMD patients, suggesting that mutation-dependent clinical features may not be present. (Optom Vis Sci 2012;89:684–691)

Key Words: electroretinography, optical coherence tomography, genetics, retinal disorder, macular degeneration, mutation analysis

Occult macular dystrophy (OMD), first described in 1989,[1] is a rare autosomal dominant macular disorder characterized by slowly progressive loss of visual acuity, normal ophthalmoscopic and fluorescein angiographic findings, and normal responses on full-field electroretinography (ERG),[2] but reduced amplitude of focal macular ERG or multifocal ERG.[2,3] In addition to autosomal dominant cases, however, patients with sporadic OMD have also been reported.[3,4] Optical coherence tomography (OCT) findings has revealed outer retinal structural abnormalities at the foveal areas in both autosomal dominant and sporadic OMD patients.[5–8] However, no gene mutation was found in any type of OMD until 2010.

In 2010, a molecular basis of autosomal dominant OMD was first elucidated: two heterozygous missense mutations (p.R45W and p.W960R) in the *RP1L1* gene were identified in four Japanese families, one of which (p.R45W) was found in three of the four families.[9] However, since the discovery of these two *RP1L1* mutations, clinical features of *RP1L1*-associated OMD have not been subsequently described.

Here, we performed mutation analysis of the *RP1L1* gene in Japanese patients with OMD. We identified the clinical features of two patients (a female proband and her mother) in a two-generation family with autosomal dominant OMD who carried the *RP1L1* mutation (p.R45W) heterozygously.

METHODS

The study was approved by the institutional review board of The Jikei University School of Medicine. The protocol adhered to the

*MD, PhD
†MD
Department of Ophthalmology (TH, TG, KK, YO, HT), Department of Molecular Genetics, Institute of DNA Medicine (HY), The Jikei University School of Medicine, Tokyo, Japan, and Tanaka Eye Clinic, Tokyo, Japan (IT).

tenets of the Declaration of Helsinki, and informed consent was obtained from all participants.

Clinical Studies

We investigated the ophthalmic features of two patients in a two-generation Japanese family (JU#0090) with autosomal dominant OMD: a female proband (II-1) and her mother (I-2) (Fig. 1A). Both the proband and her mother underwent a comprehensive ophthalmic examination, including decimal best-corrected visual acuity (BCVA), slitlamp biomicroscopy, dilated ophthalmoscopy, and fluorescein angiography (FA). For retinal scan images, the spectral domain OCT (SD-OCT) (Cirrus HD-OCT; Carl Zeiss Meditec AG, Dublin, CA) was performed using the HD 5 line raster scan protocol and Macular Cube protocol (512 × 128 scan), in which a 6 × 6-mm^2 area of the macula was scanned. Color vision was mono-ocularly evaluated using the Ishihara test (38-plate edition) and the Farnsworth Panel D-15 (Panel D-15). Visual fields were assessed using a Humphrey Field Analyzer (HFA; Carl Zeiss Meditec, Dublin, CA) with the central 30-2 threshold program, and mean deviation (MD) and corrected pattern standard deviation (CPSD) were evaluated. Full-field ERG and multifocal ERG were performed according to the protocols of the International Society for Clinical Electrophysiology of Vision. The procedure and conditions for full-field ERG and multifocal ERG recording have been detailed previously.[10,11] Data analysis of multifocal ERG was performed using the Visual Evoked Response Imaging System (Electro Diagnostic Imaging Inc., San Mateo, CA).

Focal macular ERG findings were recorded using an infrared fundus camera with a stimulus light and background illumination (ER-80; Kowa Company, Tokyo, Japan). The size of the stimulus spot, placed on the macula, was alternated between 5, 10, and 15° in diameter, and the position was confirmed via the infrared fundus monitor. The stimulus and background illumination were generated by white light-emitting diodes with peak spectra of 440 to 460 nm and 540 to 580 nm, respectively. The luminances of the stimulus light and background were 30 and 1.5 cd/m^2. The duration of the stimulation was 100 ms, and responses were amplified and filtered using digital band-pass filters from 5 to 500 Hz (Neuropack μ, MEB-9102; Nihonkoden, Tokyo, Japan). Two to three hundred responses were averaged with a stimulus frequency of 5 Hz.

Molecular Genetic Studies

A total of seven unrelated index probands (one autosomal dominant and six sporadic patients) were clinically diagnosed with OMD at the Jikei University Hospital between April 2001 and March 2007. Genomic DNA was extracted from venous blood samples using a Puregene Blood DNA Isolation kit (Gentra Systems, Minneapolis, MN), and all seven probands underwent molecular analysis. All coding exons (exon 2 to exon 4) of the *RP1L1* gene were amplified via polymerase chain reaction (PCR) using previously reported primers,[12] all of which were produced by Operon Biotechnologies (Tokyo, Japan). The PCR products were purified with a QIAquick PCR Purification kit (Qiagen, Tokyo, Japan) and used as the template for sequencing. Both strands were sequenced on an automated sequencer (3730xl DNA Analyzer; Applied Biosystems, Foster City, CA) using a BigDye Terminator kit V3.1 (Applied Biosystems).

RESULTS

Clinical Findings

The Japanese family (JU#0090) examined in this study included three members with autosomal dominant OMD (Fig. 1A).

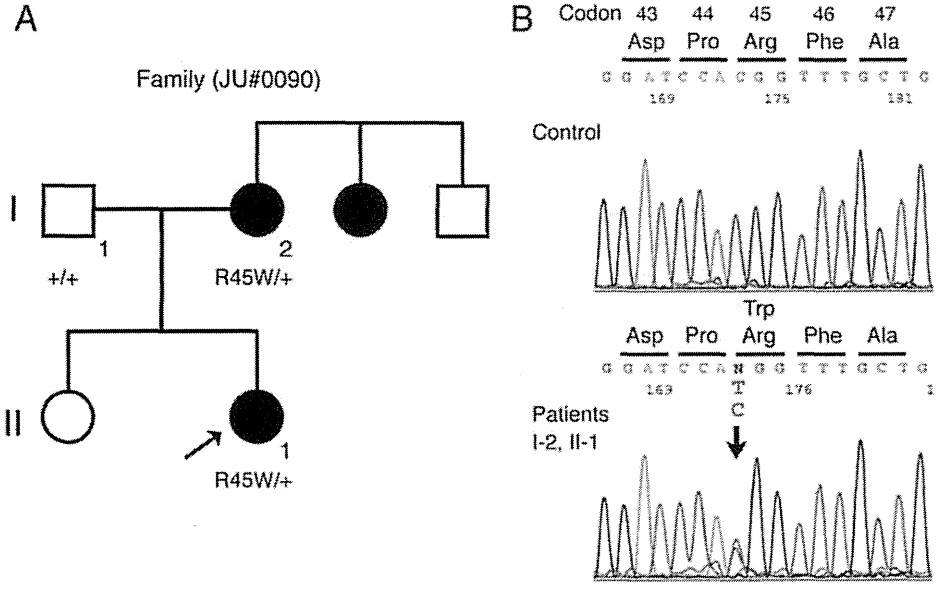

FIGURE 1.

Pedigree of Japanese family JU#0090 and sequence analysis of exon 2 of *RP1L1*. (A) Affected family members are represented by solid circles (females), with an arrow indicating the proband (patient II-1). (B) The arrow indicates the position of the altered nucleotide which resulted in a heterozygously missense mutation (p.R45W) in both patients (I-2 and II-1).

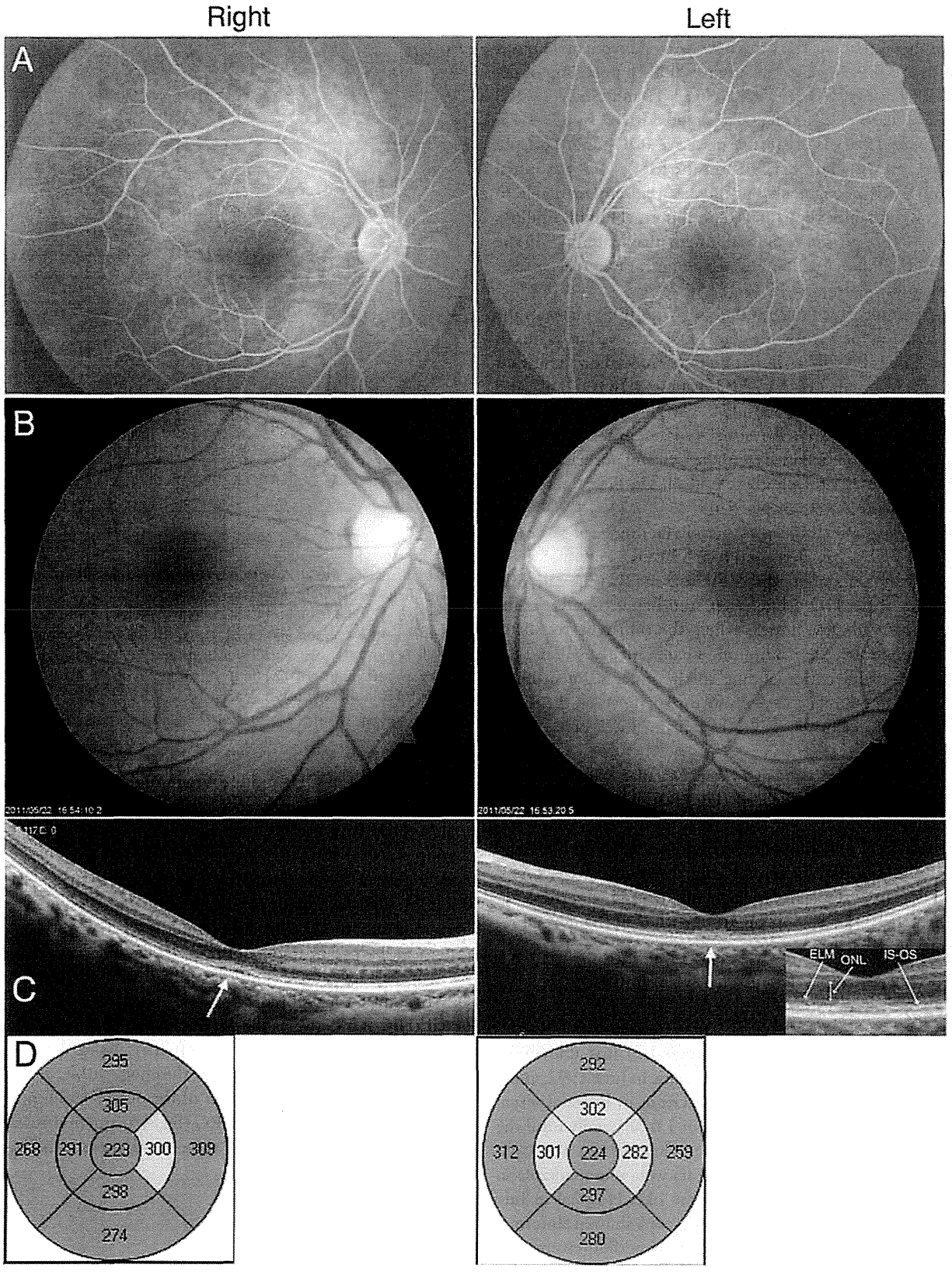

FIGURE 2.

Fluorescein angiograms, fundus photographs, and OCT findings in patient II-1. (A) Late-phase fluorescein angiograms showed unremarkable findings in the maculae but subtle hyperfluorescence along the vascular arcades due to a window defect at the age of 27 years. (B) Fundus photographs showed unremarkable findings at the age of 36 years. (C) OCT images of the HD 5 line raster scan showed outer retinal abnormalities only at the foveal areas where the thin reflective band corresponding to the ELM and the hyperreflective band corresponding to the IS/OS boundary are disorganized (arrows); however, the thickness of the ONL was well preserved at the age of 36 years. (D) The macular thickness map of the Macular Cube protocol showed normal macular thickness.

Patient II-1

The proband (patient II-1) was a 27-year-old woman who was referred to the Jikei Hospital in August 2002 complaining of decreased visual acuity. Her BCVA had been 1.0 in both eyes (OU) until the age of 20 years but had deteriorated to 0.7 (sph: −1.75, cyl: −0.25, and axis: 100°) in the right eye (OD) and 0.6 (sph: −2.25, cyl: −0.25, and axis: 130°) in the left eye (OS) at initial evaluation. Anterior segments and media were unremarkable in either eye. Ophthalmoscopy showed no abnormal fundus findings in either eye. Late phase FA showed unremarkable findings in the maculae but subtle hyperfluorescence along the vascular arcades due to a window defect in OU (Fig. 2A).

The patient identified 6/25 (OD) and 4/25 (OS) plates in the Ishihara test, and the Farnsworth Panel D-15 showed no errors in either eye. The HFA pattern deviation plots showed no significant defects, with MD values of −1.77 (OS) and −2.18 (OD) dB, and the CPSD values were 1.85 (OS) and 0.59 (OD) dB (Fig. 3A). The full-field ERG demonstrated normal rod responses in the OD (reliable data were not obtained from the OS) and normal standard combined responses, and photopic and 30-Hz flicker responses were slightly reduced in OU (Fig. 4A).

Nine years later after initial presentation (at the age of 36 years), the patient's BCVA had decreased to 0.4 in OU. Although ophthalmoscopy showed unremarkable findings in OU (Fig. 2B), SD-OCT images of the HD 5 line raster scan revealed outer retinal abnormalities at the foveal areas where the thin reflective band corresponding to the external limiting membrane (ELM) and the hyperreflective band corresponding to the inner segment-outer segment (IS/OS) boundary were disorganized; however, the thickness of the outer nuclear layer (ONL) remained well preserved in OU (Fig. 2C).

The macular thickness map of the Macular Cube protocol showed normal macular thickness (Fig. 2D). The focal macular ERG demonstrated non-detectable responses at 5°, severely reduced responses at 10°, and reduced responses at 15° in OU (Fig. 4B). In multifocal ERG, the central (ring 1) responses were absent, paracentral (ring 2) responses were greatly reduced, and the outer waveforms (rings 3 to 5) were about one-third of the normal responses in OU (Fig. 4C).

Patient I-2

The proband's affected mother (patient I-2) first underwent ophthalmic examination at Tanaka Eye Clinic in June 1992, at the age of 49 years, after experiencing a decrease in bilateral visual acuity. Although she had had a BCVA of 1.0 bilaterally until the age of 30 years, her BCVA at initial evaluation was 0.6 (sph: +0.50), and anterior segments and media were unremarkable in OU. She was subsequently referred to the Jikei Hospital in July 1992 for further examination. Ophthalmoscopy showed abnormal macular ring reflex, and FA revealed small, hyperfluorescent dots due to retinal pigment epithelium alterations in both maculae (Fig. 5A).

Goldmann perimetry conducted at the age of 51 years demonstrated bilateral central scotomas (I-1 targets) within 5 to 7° of point of fixation. The Farnsworth Panel D-15 was arranged in a deutan pattern in each eye. By the age of 56 years, her BCVA had decreased to 0.4 in OU, and HFA pattern deviation plots showed central visual field defects: MD values were +1.95 (OS) and +1.74 (OD) dB, and CPSD values were 2.81 ($p < 10\%$) (OS) and 2.56 ($p < 10\%$) (OD) dB (Fig. 3B).

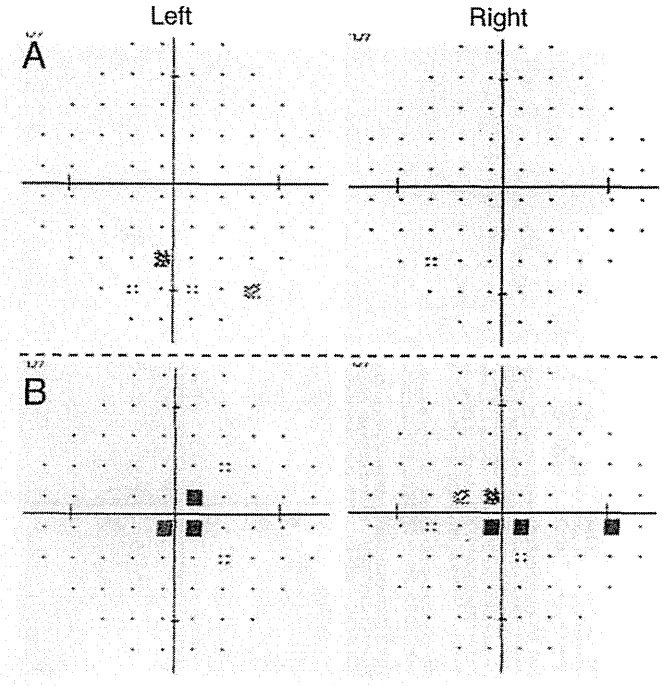

FIGURE 3.
Visual fields using the HFA with the central 30-2 threshold program. (A) No significant visual field defects were detected. MD was −1.77 (left eye) and −2.18 dB (right eye), and CPSD was 1.85 (left eye) and 0.59 dB (right eye) in patient II-1 at the age of 27 years. (B) Central visual field defects were detected. MD was +1.95 (left eye) and +1.74 dB (right eye), and CPSD was 2.81 dB ($p < 10\%$) (left eye) and 2.56 dB ($p < 10\%$) (right eye) in patient I-2 at the age of 56 years.

At the age of 70 years, her BCVA had decreased to 0.3 (OD) and 0.2 (OS). Ophthalmoscopy showed subtle retinal pigment epithelium mottling in OU (Fig. 5B). The SD-OCT of the HD 5 line raster scan showed thinning of the ONL and discontinuous reflectivity of the ELM and IS/OS lines at the foveal areas in OU (Fig. 5C). In addition, a hyporeflective zone (described elsewhere[13]) was noted (Fig. 5C) between the IS/OS line and the hyperreflective retinal pigment epithelium/choriocapillaris band. The macular thickness map showed significant thinning within the 1- and 3-mm rings and normal thickness of the outer (3 to 6 mm) ring (Fig. 5D) bilaterally. Full-field ERG (Fig. 4A) and multifocal ERG (Fig. 4C) examinations revealed the same abnormal findings as in patient II-1.

Molecular Genetic Findings

Mutation analysis of the *RP1L1* gene revealed that only patient II-1 in JU#0090 (one of the seven unrelated probands) had a heterozygous variant (c.133C>T in exon 2). This variant results in the substitution of tryptophan (TGG) for arginine (CGG) at amino acid position 45 (Fig. 1B). This missense mutation (p.R45W) was one of the two mutations previously reported in the